Supplemental Material

S1 Weathering reduction associated with an increase in organic carbon burial

What is the impact of increased organic carbon burial on weathering and $p\text{CO}_2$? The following reasoning might at first glance appear sound. Utilizing the traditional carbon isotope mass balance (Equation S1):

$$\delta^{13}\text{C}_{\text{in}} = \delta^{13}\text{C}_{\text{carb}} - f_{org} * \epsilon \tag{S1}$$

Then, applying $\delta^{13}\text{C}_{\text{in}} = -5‰$, $\epsilon = 25‰$, and an organic carbon burial fraction (f_{org}) of 0.2 gives the canonical value of 0 ‰. Increasing f_{org} from 0.2 to 0.6 yields a value of +10 ‰. Hence, if during the Lomagundi Event the organic carbon burial fraction increased from 20% to 60%, then carbonate carbon burial must have decreased from 80% to 40% of the total, i.e. by 50%, thus requiring a 50% reduction in weathering.

However, this estimate is erroneous, as it does not take into account the constraints imposed by alkalinity, which imply a far greater reduction—on the order of 91%. To illustrate the underlying logic, we employ a more complete description of the carbon cycle, one which includes alkalinity (Figure S1). For the magnitudes of the fluxes we use values modified from Kump and Arthur (1): $F^{w}_{\text{volc}} = 5$, $F^{w}_{\text{carb}} = 36$, $F^{w}_{\text{sil}} = 4$, $F^{w}_{\text{org}} = 9$, and $F^{b}_{\text{org}} = 10$, $F^{b}_{\text{carb}} = 40$, all in Tmol/yr. An increase in the fraction of organic carbon burial (f) of 0.2 to 0.6 implies an increase in the burial of organic carbon (F^{b}_{org}) from 10 to 30 Tmol/yr and a commensurate reduction in the burial of carbonate carbon (F^{b}_{carb}) from 40 to 20 Tmol/yr. To balance the reduction in carbonate burial, the input of alkalinity from the weathering of silicates and carbonates ($F^{w}_{\text{sil}} + F^{w}_{\text{carb}}$) would have to decline from 40 to 20 Tmol/yr as well. But then not enough carbon is brought in to balance the total carbon output: only 18 + 9 + 5 = 32 Tmol/yr are brought in but 40 Tmol/yr

1

are removed. Thus, an additional decline in burial of carbonate and organic carbon is required, which requires another decrease in the weathering flux, and so forth. Consequently, the overall resulting reduction in weathering is far larger than the simplistic estimate of a 50% reduction.

The procedure for calculating the inputs and outputs of carbon and alkalinity, for a specified fraction of organic carbon burial, is given below. We make only three assumptions: 1) that the system is at steady-state, 2) that the only inputs of carbon into the system are from volcanism and the weathering of carbonate and organic carbon, and 3) that the only inputs of alkalinity are from the weathering of carbonate and silicate rocks.
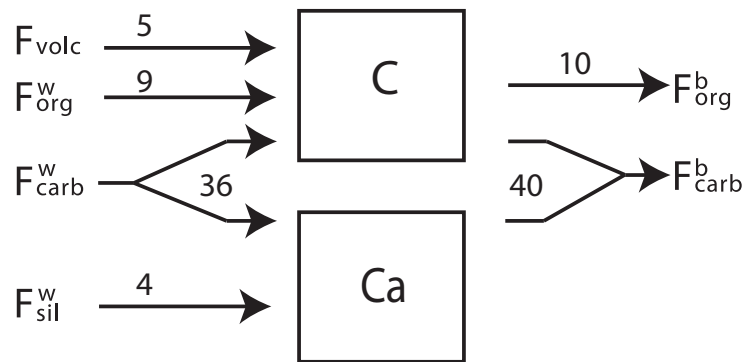

Figure S1: Basic carbon cycle model for the ocean-atmosphere carbon pool. Modified from Kump and Arthur (1). Units in Tmol/yr.

We begin by expressing the equality between the inputs and outputs of carbon that must exist at steady-state (Equation S2). We introduce a multiplier, β, which represents the decrease (or increase) in the weathering derived fluxes relative to their original steady-state values (for instance a 20% reduction would be $\beta = 0.8$). The multiplication of the weathering of organic and carbonate carbon fluxes by β indicates that they are surficial fluxes subject to physical and

chemical weathering processes, whereas volcanic carbon input is not.

$$F_{\text{volc}} + \left(F_{\text{org}}^{\text{w}} + F_{\text{carb}}^{\text{w}}\right)\beta = F_{\text{org}}^{\text{b}} + F_{\text{carb}}^{\text{b}} \tag{S2}$$

Dividing by F_{carb}^{b} gives:

$$\frac{F_{\text{volc}} + \left(F_{\text{org}}^{\text{w}} + F_{\text{carb}}^{\text{w}}\right)\beta}{F_{\text{carb}}^{\text{b}}} = \frac{F_{\text{org}}^{\text{b}}}{F_{\text{carb}}^{\text{b}}} + 1 \tag{S3}$$

The ratio of the organic to carbonate carbon burial fluxes, on the left, can be expressed in terms of the organic carbon burial fraction (f_{org}):

$$\frac{F_{\text{org}}^{\text{b}}}{F_{\text{carb}}^{\text{b}}} = \frac{f_{org}}{1 - f_{org}} \tag{S4}$$

So that:

$$\frac{F_{\text{volc}} + \left(F_{\text{org}}^{\text{w}} + F_{\text{carb}}^{\text{w}}\right)\beta}{F_{\text{carb}}^{\text{b}}} = \frac{f_{org}}{1 - f_{org}} + 1 = \frac{1}{1 - f_{org}} \tag{S5}$$

Now we take into consideration the fact that the carbonate burial flux must conserve the contribution of alkalinity from the carbonate and silicate weathering fluxes:

$$(F_{\text{carb}}^{\text{w}} + F_{\text{sil}}^{\text{w}})\beta = F_{\text{carb}}^{\text{b}} \tag{S6}$$

We substitute the alkalinity constraint back into the expression obtained from the carbon mass balance:

$$\frac{F_{\text{volc}} + \left(F_{\text{org}}^{\text{w}} + F_{\text{carb}}^{\text{w}}\right)\beta}{(F_{\text{carb}}^{\text{w}} + F_{\text{sil}}^{\text{w}})\beta} = \frac{1}{1 - f_{org}} \tag{S7}$$

Rearranging for β yields the final expression:

$$\boxed{\beta = \frac{F_{\text{volc}}}{\left(\dfrac{1}{1 - f_{org}}\right)(F_{\text{carb}}^{\text{w}} + F_{\text{sil}}^{\text{w}}) - (F_{\text{org}}^{\text{w}} + F_{\text{carb}}^{\text{w}})}} \tag{S8}$$

Substituting the values for the weathering fluxes and volcanic input allows estimating β for a given f_{org}. If we further assume $\beta = \text{RCO}_2^{0.3}$ we can estimate RCO_2, defined as the ratio of

f_{org}	$\delta^{13}C$	β	RCO_2	pCO_2
0.2	0	1	1	10,000
0.4	5	0.23	0.0075	75.3
0.6	10	0.09	0.00033	3.37
0.8	15	0.03	1.0685×10^{-5}	0.1

Table S1: Values of β calculated in accordance with Equation S8. Also shown are the corresponding $\delta^{13}C$ values (assuming the canonical values of -5 ‰ and 25 ‰ for the carbon input and photosynthetic fractionation), the RCO_2 value, and the pCO_2 value required to maintain steady-state.

48 perturbed pCO_2 to baseline pCO_2. We also include the estimated reduction in pCO_2 from a

49 baseline of 10,000 ppm.

50 As can be seen in the values in Table S1, the values of β decline precipitously as the values

51 of f_{org} increase. At high values of f_{org} (and $\delta^{13}C$), β is dramatically reduced suggesting that

52 non-physically low levels of weathering are required.

S2 Volcanic carbon inputs and organic carbon burial

54 Could a long-lived, but temporary increase in carbon inputs potentially prevent atmospheric

55 CO_2 levels from crashing, while still allowing increased organic matter burial? To estimate the

56 required increase in carbon input the following calculation might be carried out: carbon isotope

57 mass balance requires that f_{org} be equal to 0.6 for $\delta^{13}C_{carb}$ to reach + 10‰ (if epsilon is 25‰).

58 Then, assuming the total influx is composed of the initial influx (x), 20% of which is buried

59 as organic matter, and an additional influx (y), 100% of which is buried as organic matter, the

60 carbon isotope mass balance is:

$$\delta^{13}C_{in} * (x + y) = \delta^{13}C_{carb} * 0.8 * x + \delta^{13}C_{org} * 0.2 * x + \delta^{13}C_{org} * y \qquad (S9)$$

Then, substituting the values for $\delta^{13}C_{carb}$ (+10‰) and $\delta^{13}C_{org}$ (-15‰):

$$-5 * (x + y) = 10 * 0.8 * x - 15 * 0.2 * x - 15 * y \qquad \text{(S10)}$$

$$-5x - 5y = 8x - 3x - 15y \qquad \text{(S11)}$$

$$10y = 10x \qquad \text{(S12)}$$

$$y = x \qquad \text{(S13)}$$

So a doubling of the total carbon input is implied, i.e.:

$$\frac{y}{y + x} = 2 \qquad \text{(S14)}$$

However, this calculation, similarly to the calculation presented in the opening to Section S1, fails to take into account the constraints imposed by alkalinity. Using the framework presented in S1 we can carry out a more refined calculation and show the difficulty with this proposed solution. We include an additional carbon flux to the mass balance so that it becomes:

$$\frac{F_{volc} + F_{extra} + \left(F_{org}^w + F_{carb}^w\right)\beta}{\left(F_{carb}^w + F_{sil}^w\right)\beta} = \frac{1}{1 - f_{org}} \qquad \text{(S15)}$$

The magnitude of F_{extra} should be large enough so that no reduction in weathering occurs ($\beta \geq$ 1), and it must also honor the isotopic constraints which suggest that 60% of incoming carbon was buried as organic carbon ($f_{org} = 0.6$). Using the same values for the fluxes as in Section S1 (F_{volc} = 5; F_{wcarb} = 36; F_{worg} = 9; F_{wsil} = 4, all in Tmol/yr), substituting $\beta = 1$ and $f_{org} = 0.6$, and then solving for F_{extra} yields:

$$\frac{5 + F_{extra} + 9 + 36}{36 + 4} = \frac{1}{1 - 0.6} \qquad \text{(S16)}$$

$$\frac{50 + F_{extra}}{40} = 2.5 \qquad \text{(S17)}$$

5

$$F_{\text{extra}} = 50 \quad \text{Tmol/yr} \tag{S18}$$

So, the results indicate that 50 Tmol/yr of extra carbon are required, an amount that is equal to the total baseline input flux of carbon ($F_{\text{volc}} + F_{\text{wcarb}} + F_{\text{worg}}$). Thus, this calculation indicates that a doubling of the total input flux of carbon is required, exactly as indicated by the simple calculation above, but now the difficulty becomes apparent: the extra carbon has to be supplied in "volcanic" form, that is as CO_2 and not HCO_3^- or CO_3^{2-}. The reason is that carbon in the form of carbonate alkalinity ($HCO_3^- + CO_3^{2-}$), such as supplied by the weathering of calcium silicates and carbonates, is already tied to burial of carbonates and thus is unavailable for organic carbon burial (or at least without causing an imbalance in alkalinity and a decline in $p\text{CO}_2$). An increase in the organic carbon weathering flux is also out of the question since it would simply undo the ^{13}C enrichment effected by the elevated organic carbon burial. Consequently, an eleven-fold increase in volcanism is required (from 5 to 55 Tmol/yr), and not simply a two fold increase in total carbon input. This required increase in volcanic input is very large, and, even if such an increase were geologically plausible, it would only solve half the problem: an increase in volcanic CO_2 input would resolve the conundrum of CO_2 deficit, but not answer the difficulty of O_2 accumulation. Thus, other sources of CO_2 which also consume O_2, such as siderite and sulfide oxidation, must be seriously considered.

S3 Organic carbon burial accompanied by pyrite oxidation

An increase in organic carbon burial, unaccompanied by increased carbon input, leads to non-physically low levels of weathering because of the resulting imbalance in alkalinity. Pyrite oxidation can ameliorate this imbalance by supplying acidity, thus bolstering $p\text{CO}_2$ levels. As stated in the main text, both the acidification of limestones by sulfuric acid and the sulfuric acid

weathering of silicates equally lead to the release of carbon dioxide. The former acts by direct

conversion of carbonate to CO_2, while the latter by replacing carbonic acid weathering with

sulfuric acid weathering and thus allowing volcanic CO_2 to go un-consumed. Consequently,

the resulting CO_2 is available for organic carbon burial without any charge balance constraints,

in contrast to carbonate alkalinity ($[HCO_3^-], [CO_3^{2-}]$). It is, nonetheless, important to note that

the supply of carbon from the sulfuric acid weathering of silicates should not exceed the flux of

volcanic carbon that would otherwise exit as $CaCO_3$ (4 Tmol/yr). Acidification of Ca-silicates

in excess of this quantity would lead to an increase in $CaCO_3$ burial and a decrease in the $\delta^{13}C$

of the ocean-atmosphere system.

To constrain the required fluxes we augment our previous carbon cycle model with a sulfate

box, with one input flux of sulfate from pyrite oxidation and one output flux of $CaSO_4$ (Figure
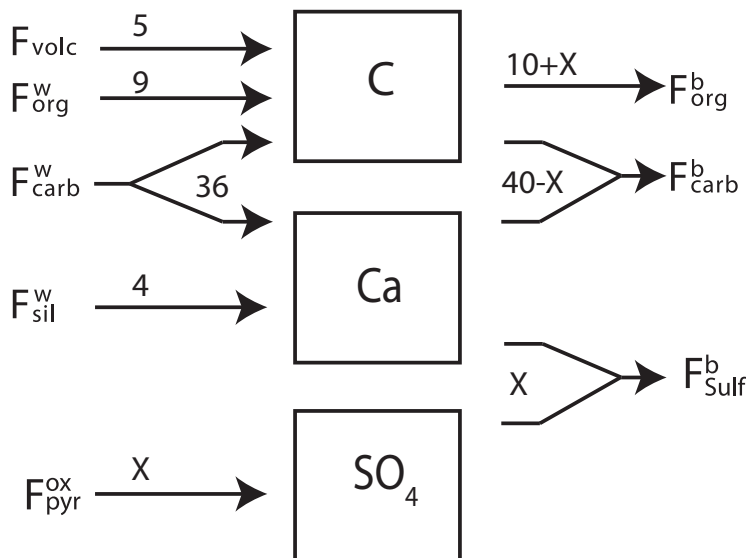S2):

Figure S2: Basic carbon cycle model for the ocean-atmosphere carbon pool with a sulfate box. X is the variable pyrite oxidation flux. Modified from Kump and Arthur (1). Units in Tmol/yr.

We start with the three mass balance equations, one for each element:

$$C: \quad F_{volc} + F_{org}^w + F_{carb}^w = F_{org}^b + F_{carb}^b \tag{S19}$$

$$Ca: \quad F_{sil}^w + F_{carb}^w = F_{carb}^b + F_{sulf}^b \tag{S20}$$

$$S: \quad F_{pyr}^{ox} = F_{sulf}^b \tag{S21}$$

Rearranging we get:

$$F_{sil}^w + F_{carb}^w - F_{pyr}^{ox} = F_{carb}^b \tag{S22}$$

Dividing by F_{carb}^b

$$\frac{F_{volc} + F_{org}^w + F_{carb}^w}{F_{carb}^b} = \frac{1}{1-f} \tag{S23}$$

And substituting back into the expression for carbon:

$$\frac{F_{volc} + F_{org}^w + F_{carb}^w}{F_{sil}^w + F_{carb}^w - F_{pyr}^{ox}} = \frac{1}{1-f} \tag{S24}$$

Then isolating the oxidation flux of pyrite gives:

$$F_{pyr}^{ox} = (F_{sil}^w + F_{carb}^w) - (1-f)(F_{volc} + F_{org}^w + F_{carb}^w) \tag{S25}$$

We can then calculate the necessary pyrite oxidation fluxes required to balance the burial of organic carbon by removal of calcium as gypsum (Table S2):

f	$\delta^{13}C$	F_{pyr}^{ox}	O_2 imbalance
0.2	0	0	0
0.3	2.5	5	-4.375
0.4	5	10	-8.75
0.6	10	20	-17.5
0.8	15	30	-26.25
1	20	40	-35

Table S2: Pyrite oxidation flux required to balance elevated organic carbon burial, in Tmol/yr. The O_2 imbalance is the extra O_2 required for pyrite oxidation beyond that which is produced by organic carbon burial, in Tmol/yr.

As an example of how pyrite oxidation makes CO_2 available for organic carbon burial, consider the end-member case where $f = 1$, i.e. all the carbon coming in is buried as organic carbon and none as carbonate carbon. In this case carbonic acid weathering of silicates and carbonates must be zero. For pCO_2 to remain elevated, carbonic acid weathering must be replaced by sulfuric acid weathering. Thus, a $SO_4^=$ flux of 40 Tmol/yr, with 4 coming from sulfuric acid weathering of Ca-silicates and 36 from acidification of carbonates completely compensates for missing carbonic acid weathering. Now, 40 Tmol/yr of Ca that would otherwise exit as $CaCO_3$ get buried as gypsum (or accumulate in the ocean), making available for organic carbon burial 40 Tmol/yr of carbon. The only remaining problem is that pyrite oxidation requires 15/8*40 = 75 Tmol/yr of O_2, which is 35 Tmol/yr more than organic carbon burial can supply.
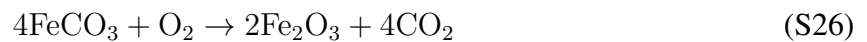
It is pertinent to note that the oxygen deficit would be even more severe if sulfide oxidation and carbonate dissolution occurred without a concomitant increase in organic carbon burial. In the framework of the above example 75 Tmol/yr of O_2 would be consumed and not just 35 Tmol/yr. Consequently, the oxygen imbalance which arises during sulfide oxidation argues against recent claims for sulfide oxidation as a long-term source of carbon (2). And, if sulfide oxidation did make a significant contribution of carbon during Himalayan uplift, as argued by Torres et al. (2), it would have driven a substantial drop in pO_2 during the Cenozoic, something for which there is no evidence.

S4   Siderite Oxidation and $\delta^{13}C$
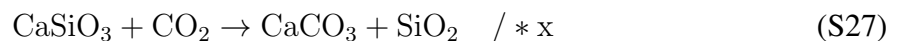
Siderite oxidation can be called upon as a source of carbon over geologic timescales since, in contrast to sulfide oxidation, it produces more CO_2 than it consumes O_2 (Equation S26) and so can supply CO_2 in excess of the amount that is required by organic carbon burial to keep the process going. However, in the context of the Lomagundi Event, the oxidation of siderite

9

must have also been coupled to processes that produce acidity (sulfide oxidation) or consume O_2 (iron silicate oxidation) as siderite oxidation alone together with the simple (carbonic acid) weathering silicates could not have generated the Lomagundi Event. The reason is that the alkalinity generated during the consumption of the excess carbon by silicate weathering would have negated the ^{13}C enrichment effected by organic carbon burial.

To appreciate this difficulty, and more generally, some of the intricacies of siderite oxidation, consider the oxidation of siderite coupled to weathering of silicates and the burial of organic carbon and carbonate carbon:
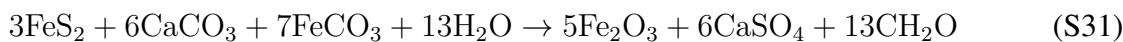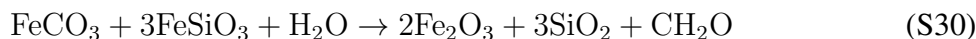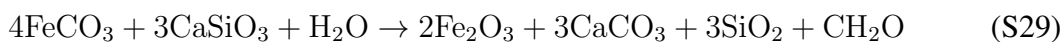
$$4FeCO_3 + O_2 \rightarrow 2Fe_2O_3 + 4CO_2 \tag{S26}$$

$$CaSiO_3 + CO_2 \rightarrow CaCO_3 + SiO_2 \quad / * x \tag{S27}$$

$$CO_2 + H_2O \rightarrow CH_2O + O_2 \quad / * y \tag{S28}$$

One could combine these equations in two ways: first, as an overall CO_2-neutral reaction ($x + y = 4$), and second, as an O_2-neutral reaction ($y = 1$). Together with the constraints from the carbon isotope record ($f_{org} = y/(y + x) = 0.6$) one can obtain the desired stoichiometries. In the O_2 neutral case $y = 1$ and $x = 2/3$, and in the CO_2 neutral case $x = 1.6$ and $y = 2.4$. Hence, the CO_2-neutral reaction leads to net release of O_2 at a rate of 1.4 moles of O_2 per 4 moles of siderite oxidized, while the O_2 neutral reaction leads to net release of CO_2, at a rate of 2 1/3 moles per 4 moles of siderite oxidized.

These imbalances cannot be maintained over timescales of hundreds of m.y. of years over which the Lomagundi Event occurs. In the CO_2 neutral reaction one is left with with a large excess of O_2, and in the O_2 neutral reaction case one is left with a large excess of CO_2. The duration of the event is such that if the organic carbon burial were not fully compensated in terms of both CO_2 and O_2 physically non-permissible atmospheric compositions would quickly arise (i.e. pO_2

10

$_{157}$ or $p\text{CO}_2 \gg 1$ atm). Thus, CO_2 or O_2 must not appear in the overall reaction for oxidation of

$_{158}$ siderite together with the weathering of calcium silicates; nor for that matter should they appear

$_{159}$ in any other reaction which is postulated to have taken place over the duration of the Lomagundi

$_{160}$ Event. Below we give the appropriate reactions for siderite oxidation coupled to calcium silicate

$_{161}$ weathering, siderite oxidation coupled to Fe-silicate weathering, and siderite oxidation coupled

$_{162}$ to Fe-sulfide oxidation and acidification of carbonates.

$$4\text{FeCO}_3 + 3\text{CaSiO}_3 + \text{H}_2\text{O} \rightarrow 2\text{Fe}_2\text{O}_3 + 3\text{CaCO}_3 + 3\text{SiO}_2 + \text{CH}_2\text{O} \qquad \text{(S29)}$$

$_{163}$

$$\text{FeCO}_3 + 3\text{FeSiO}_3 + \text{H}_2\text{O} \rightarrow 2\text{Fe}_2\text{O}_3 + 3\text{SiO}_2 + \text{CH}_2\text{O} \qquad \text{(S30)}$$

$_{164}$

$$3\text{FeS}_2 + 6\text{CaCO}_3 + 7\text{FeCO}_3 + 13\text{H}_2\text{O} \rightarrow 5\text{Fe}_2\text{O}_3 + 6\text{CaSO}_4 + 13\text{CH}_2\text{O} \qquad \text{(S31)}$$

$_{165}$ What are the biggest differences between the three reactions? Examine the first reaction above

$_{166}$ (Equation S29): the 1 mol of oxygen produced during the burial of organic matter is balanced

$_{167}$ by the oxidation of 4 moles of siderite which produces 4 moles of CO_2. One mole of the 4

$_{168}$ moles of CO_2 which is produced goes to the burial of organic carbon while the other 3 to the

$_{169}$ weathering of silicates. The overall result is an f_{org} ratio of 0.25. Thus, this reaction is nearly

$_{170}$ isotopically transparent. The increase in the burial of organic carbon in this case is balanced by

$_{171}$ an increase in the burial of carbonate carbon at a ratio that is very near the long term average

$_{172}$ $\delta^{13}\text{C}$ of the exogenic cycle. Such a reaction would have contributed little to ^{13}C enrichment

$_{173}$ during the Lomagundi Event, and even then mostly via the relatively heavy $\delta^{13}\text{C}$ value of the

$_{174}$ siderite carbon. Contrast Equation S29 with Equations S30 and S31. In the latter two reactions

$_{175}$ the burial of organic carbon is not accompanied by the offsetting burial of carbonates making

$_{176}$ them much more effective in driving ^{13}C enrichment.

$_{177}$ Thus, there are more and less efficient ways to drive ^{13}C enrichment via siderite oxidation cou-

$_{178}$ pled to organic carbon burial. When inverting the $\delta^{13}\text{C}$ record, one is given a degree of freedom

11

in choosing the varying proportions of the three reactions. By choosing a large proportion of siderite oxidation coupled to non-Fe-silicate weathering (Equation S29) one could explain the Lomagundi Event in a way that involves an amount of reactants that exceeds those which were likely available for oxidation or leads to the production of more products than can be accounted for.

Does such a worst-case-scenario calculation does invalidate the hypothesis? No, it is the best case scenario which is the test: if it can be shown that even under the most propitious circumstances the hypothesis fails, then it can be confidently rejected. Hence, in our tables and model runs below we focus on the most effective ways to drive the Lomagundi Event and show that these do not violate mass balance constraints. We do not claim that back reactions (sulfide burial, oxidation of organic carbon) or the weathering of non-Fe-silicates did not occur, but we do maintain that these must have been minor in relation to the forward reactions, as demanded by constraints imposed by the global mass balance on the one hand and the δ^{13}C (and δ^{34}S) record on the other.

S5   Derivation of Equation 10

We can use Equations S30 and S31 to construct a carbon isotopic mass balance. We assume that some fraction, α, of the siderite is oxidized together with Fe-silicates according to Equation S30, and the rest, $(1 - \alpha)$, reacts with sulfides and carbonates according to Equation S31. The first reaction (Equation S30) implies that the burial of organic carbon occurs at a 1:1 ratio with siderite oxidation, such that a certain portion of organic carbon burial is proportional to the siderite oxidation flux associated with iron silicate oxidation. Following the same logic, the stoichiometry of the second reaction is such that for every mol of siderite oxidized, 6/7 mol of carbonate are acidified and 13/7 mol of organic carbon are buried, inducing the following

12

isotopic mass balance:

$$(1-\alpha)F_{sid}^{w}\,\delta_{sid}^{w}\,+\,\frac{6}{7}(1-\alpha)F_{sid}^{w}\,\delta_{carb}^{w}\,=\,\frac{13}{7}(1-\alpha)F_{sid}^{w}\,\delta_{org}^{b} \tag{S32}$$

Adding the above expressions to the mass balance of the pre-Lomagundi carbon cycle,

$$F_{in}^{w,0}\,\delta_{in}^{w,0}\,=\,F_{carb}^{b,0}\,\delta_{carb}^{b}\,+\,F_{org}^{b,0}\,\delta_{org}^{b} \tag{S33}$$

gives:

$$F_{in}^{w,0}\,\delta_{in}^{w,0}+\alpha\,F_{sid}^{w}\,\delta_{sid}^{w}\,+\,(1-\alpha)F_{sid}^{w}\,\delta_{sid}^{w}\,+\,\frac{6}{7}(1-\alpha)F_{sid}^{w}\,\delta_{carb}^{w}$$
$$=\,F_{carb}^{b,0}\,\delta_{carb}^{b}\,+\,F_{org}^{b,0}\,\delta_{org}^{b}\,+\,\alpha\,F_{sid}^{w}\,\delta_{org}^{b}\,+\,\frac{13}{7}(1-\alpha)F_{sid}^{w}\,\delta_{org}^{b}$$

We assume that the isotopic composition of all the organic carbon burial is fractionated by a constant amount relative to seawater, so given by $(\delta_{carb}^{b}-\epsilon)$, where ϵ is the photosynthetic fractionation. Collecting terms gives the following mass balance equation:

$$F_{in}^{w,0}\,\delta_{in}^{w,0}\,+\,F_{sid}^{w}\left[\delta_{sid}^{w}\,+\,\frac{6}{7}(1-\alpha)\,\delta_{carb}^{w}\right]\,=\,F_{carb}^{b,0}\,\delta_{carb}^{b}\,+\,\left[F_{org}^{b,0}\,+\,\left(\frac{13}{7}-\frac{6}{7}\alpha\right)F_{sid}^{w}\right](\delta_{carb}^{b}-\epsilon) \tag{S34}$$

Rearranging so that it is given for $\delta^{13}C$ of the ocean-atmosphere system:

$$\delta_{carb}^{b}\,=\,\frac{F_{in}^{w,0}\,\delta_{in}^{w,0}\,+\,F_{sid}^{w}\left[\delta_{sid}^{w}\,+\,\frac{6}{7}(1-\alpha)\,\delta_{carb}^{w}\right]\,+\,\epsilon\left[F_{org}^{b,0}\,+\,\left(\frac{13}{7}-\frac{6}{7}\alpha\right)F_{sid}^{w}\right]}{F_{org}^{b,0}\,+\,F_{carb}^{b,0}\,+\,\left(\frac{13}{7}-\frac{6}{7}\alpha\right)F_{sid}^{w}} \tag{S35}$$

Note that:

$$F_{in}^{w,0}\,=\,F_{org}^{b,0}\,+\,F_{carb}^{b,0} \tag{S36}$$

and

$$F_{in}^{w,0}\,\delta_{in}^{w,0}\,=\,F_{org}^{b,0}(\delta_{carb}-\epsilon)\,+\,F_{carb}^{b,0}\delta_{carb}^{b} \tag{S37}$$

so that assuming $\delta_{carb}^{w,0}=0\,\text{‰}$ gives:

$$F_{in}^{w}\,\delta_{in}\,+\,F_{org}^{b}\,\epsilon\,=\,0 \tag{S38}$$

13

Thus:

$$\delta_{\text{carb}}^{\text{b}} = \frac{F_{\text{in}}^{\text{w},0}\,\delta_{\text{in}}^{\text{w},0} + \epsilon\,F_{\text{org}}^{\text{b},0} + F_{\text{sid}}^{\text{w}}\left[\delta_{\text{sid}}^{\text{w}} + \left(\frac{13}{7} - \frac{6}{7}\alpha\right)\epsilon\right]}{F_{\text{in}}^{\text{w}} + \left(\frac{13}{7} - \frac{6}{7}\alpha\right)F_{\text{sid}}^{\text{w}}} \tag{S39}$$

and finally:

$$\delta_{\text{carb}}^{\text{b}} = \frac{F_{\text{sid}}^{\text{w}}\left[\delta_{\text{sid}}^{\text{w}} + \epsilon\left(\frac{13}{7} - \frac{6}{7}\alpha\right)\right]}{\left(F_{\text{in}}^{\text{w}} + \left(\frac{13}{7} - \frac{6}{7}\alpha\right)F_{\text{sid}}^{\text{w}}\right)} \tag{S40}$$

To make the expression more compact we define an alpha prime:

$$\alpha' = \frac{13}{7} - \frac{6}{7}\alpha \tag{S41}$$

So the final expression is:

$$\boxed{\delta_{\text{carb}}^{\text{b}} = \frac{F_{\text{sid}}^{\text{w}}\left[\delta_{\text{sid}}^{\text{w}} + \epsilon\,\alpha'\right]}{F_{\text{in}}^{\text{w}} + \alpha'\,F_{\text{sid}}^{\text{w}}}} \tag{S42}$$

Equation 10 in the main text (or Equation S42 above) has a Michaelis-Menten form (as is borne out in Figure 2: as the value of $F_{\text{sid}}^{\text{w}}$ increases, $\delta_{\text{carb}}^{\text{b}}$ asymptotically approaches the value of $\frac{\delta_{\text{sid}}^{\text{w}}}{\alpha'} + \epsilon$, which is approximately 24 ‰. When the siderite flux is zero, the carbon isotopic composition of the ocean-atmosphere system returns to its long-term steady-state value of 0‰.

S6 Global mass balance

Using Equation S42 it is further possible to calculate the siderite oxidation flux required by a Gaussian shaped positive excursion of up to +10 ‰ of a given duration (Figure S3). The total siderite flux is then given by the area under the $F_{\text{sid}}^{\text{w}}$ curve.

To calculate an alpha, we use a constrained optimization algorithm (*fmincon*, Matlab (3)), such that a minimum amount of siderite is used, coupled to the constraint that the total integrated oxidation of pyrite not exceed the total exogenic sulfur pool of 534 Emol of sulfur. The logic behind this choice is that the total amount of exogenic sulfur, which is currently partitioned
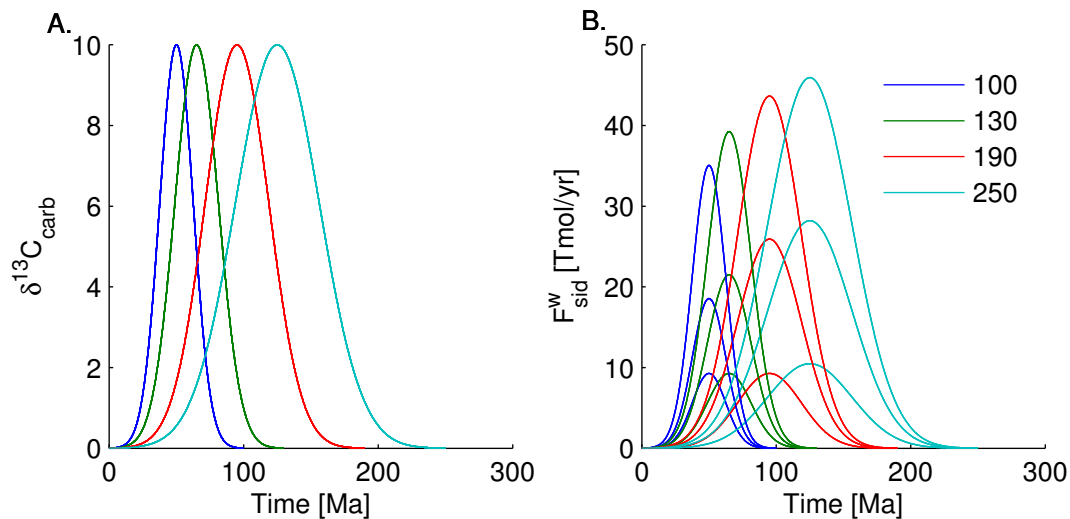
14

Figure S3: A. Gaussian shaped positive δ^{b}_{carb} excursions up to +10 ‰ with durations of 100, 130, 190, and 250 m.y. B. The resulting siderite oxidation flux according to Equation S42, with the values of alpha set to keep the total sulfate production below 534 Emol. Area under curves given in Table S3. Different colored curves in both plots correspond to different durations.

228 between the ocean, continental sulfide, and continental sulfate, likely existed entirely as con-

229 tinental sulfide prior to the Lomagundi event, and was thus available for oxidation during the

230 event. We do not claim that all the sulfur was oxidized and precipitated as gypsum. Rather,

231 we utilize this constraint as an upper theoretical bound on the extent of siderite oxidation via

232 Equation S31.

233 The results are given in Table S3 for four durations (100, 130, 190, and 250 m.y.) and three

234 input fluxes (25, 50, and 75 Tmol/yr). The code to produce the figure and table is given in

235 the supplementary files. We also include the cumulative amounts of reactants consumed and

236 products produced during our dynamic model runs, which are discussed in Section S7. The

237 three runs (Model 1–3) given are the same model runs that are presented in Figure S7. Positive

238 values for $CaCO_3$ in the first two runs indicate that carbonate dissolution was lower in the

239 perturbed state than in steady-state. This is due to the lower than baseline pCO_2 which occurs

in those two runs.

F_{in}^w	Duration	FeS_2	$CaCO_3$	$FeSiO_3$	$FeCO_3$	Fe_2O_3	$CaSO_4$	CH_2O	α
25 Tmol/yr	100 my	-125	-249	0	-291	208	249	540	0
25 Tmol/yr	130 my	-162	-324	0	-378	270	324	702	0
25 Tmol/yr	190 my	-237	-473	0	-552	394	473	1025	0
25 Tmol/yr	250 my	-267	-534	-593	-821	840	534	1355	0.24
50 Tmol/yr	100 my	-249	-498	0	-581	415	498	1079	0
50 Tmol/yr	130 my	-267	-534	-760	-876	952	534	1410	0.29
50 Tmol/yr	190 my	-267	-534	-2760	-1543	2285	534	2077	0.6
50 Tmol/yr	250 my	-267	-534	-4759	-2209	3618	534	2743	0.72
75 Tmol/yr	100 my	-267	-534	-1426	-1098	1396	534	1632	0.43
75 Tmol/yr	130 my	-267	-534	-2926	-1598	2396	534	2132	0.61
75 Tmol/yr	190 my	-267	-534	-5926	-2598	4396	534	3132	0.76
75 Tmol/yr	250 my	-267	-534	-8926	-3598	6396	534	4132	0.83
Model 1	130 my	-41	644	-2441	-813	1648	82	806	0.88
Model 2	130 my	-45	34	-3051	-1118	2108	91	1205	0.90
Model 3	130 my	-50	-574	-3662	-1424	2568	101	1604	0.92
Estimated crustal reservoir size (all refs)		84 – 294	2800 – 9600	2886	350 – 3000	50 / 4000	81 – 240	675 – 1700	
Garrels and Perry (4)		294	5083	–	350	263	240	1042	
Sleep (5)		170	6000	–	–	50/4000	180	1200	
Holser et al. (6)		84 – 294	3505 – 6460	–	–	–	81 – 240	930 – 1300	
Hayes and Waldbauer (7)		–	2800 – 9600	–	–	–	–	675 – 1700	
Yaroshevsky (8)		229	5790	2886	–	393/1280	318	1100	
Ronov et al. (9)		–	–	–	3000	–	–	–	

Table S3: Top: total amounts in Emol (10^{18}) of reactants consumed and products generated during a Gaussian shaped $\delta^{13}C$ excursion of up to + 10 ‰, obtained via two different calculations. First, by utilizing Equation 10 (Figure S3), together with the constraint that the amount of pyrite oxidized together with siderite (Reaction 9) did not generate sulfate in excess of the modern $CaSO_4$ + FeS_2 reservoirs (534 Emol); siderite oxidation accompanied by iron silicate oxidation (Reaction 8) was presumed to make up the remainder. Second, using the dynamic model runs, in which case runs with non-physical atmospheric chemistries ($pO_2 \gg 1$ atm and $pCO_2 \ll 0$ atm) were rejected. The three runs (Model 1–3) are the same model runs presented in Figure S7. Positive values for $CaCO_3$ in the first two runs indicate that carbonate dissolution was lower in those runs than in steady-state. In all cases the fraction of siderite accompanied by $FeSiO_3$ oxidation (Reaction 8) is given by α. Bottom: estimated reservoir sizes. All are given for the present, except for siderite which is given for 2.2 Ga. Higher Fe_2O_3 estimate includes oxidized iron in crystalline silicate rocks.

To compare the results of our calculations to measured values, we compiled estimates of relevant sedimentary reservoirs sizes. First, we give some comments on the estimates culled from the literature which are presented at the bottom of Table S3. We then discuss the degree of correspondence between our calculations and the estimates. The most detailed inventory of the

sizes of the crustal reservoirs of $CaCO_3$, C_{org}, FeS_2, and $CaSO_4$ can be found in Holser et al. (6), which also summarizes previous estimates from Holser and Kaplan (10), Li (11), Garrels and Perry (4), Schidlowski and Eichmann (12), Nielsen (13), and Garrels and Lerman (14). The reported values fall in the range of 84 – 294 Emol S for the sulfide reservoir; 81 – 240 Emol S for the sulfate reservoir; 3505 – 6460 Emol for $CaCO_3$; and 930 – 1300 Emol for C_{org}. Hayes and Waldbauer (7) give an updated and in-depth discussion, which, in addition to the values given by Holser et al., summarizes more recent values for sedimentary compilations given by Wedepohl (15), Hunt (16), Des Marais (17), Berner (18), and Arvidson et al. (19), which fall within the range of 2800 – 6500 Emol of $CaCO_3$ and 675 – 1300 Emol of C_{org}. They also cite mass-age data on carbonates from Wilkinson and Walker (20), which suggest a somewhat larger carbonate reservoir size (7900 – 9600 Emol), and thus a correspondingly larger C_{org} reservoir size (1400 – 1700).

Estimates for crustal iron are given by Yaroshevsky (8), who summarizes previous results from Vinogradov (21) and Ronov et al. (22): the sedimentary shell is estimated to contain 393.75 Emol of oxidized iron and 1018.5 Emol of reduced iron, with another 888 Emol of oxidized iron and 1867 Emol of reduced iron in the upper crust (granitic-metamorphic shell), totaling 1280 Emol of oxidized iron and 2886 of reduced iron. For oxidized iron, Garrels and Perry estimate the excess oxidized iron in sedimentary rocks at 263 Emol Fe_2O_3. Sleep (5) gives a lower estimate for sedimentary oxidized iron: 50 Emol of sedimentary Fe_2O_3, requiring 100 Emol of Fe and 25 Emol of O_2 to have been produced, but a higher estimate for oxidized crustal iron (including hard rocks) of 4000 Emol of Fe_2O_3, requiring 8000 Emol Fe and 2000 Emol O_2, though he does acknowledge that the uncertainties in composition of the lower continental crust could lead to the lower, but still very large, estimate of 2000 Emol Fe_2O_3, requiring 1000 Emol of O_2 to have been produced. Hayes and Waldbauer (7) cite Ronov and Yaroshevsky (23) for an estimate of 1020 O_2 equivalents, or 2040 Emol of Fe_2O_3, and a higher estimate

from Goldschmidt of 1860 Emol O_2 equivalents, or 3720 Emol Fe_2O_3—near the estimate of Sleep. Altogether, the estimates converge on oxidized crustal iron as being the most substantial reservoir of O_2 equivalents.

For siderite, other than the anecdotal descriptions of its relative abundance given in Ohmoto et al. (24), the only quantitative estimate is by Ronov et al. (9) based on observations of the Russian platform. At 2.3 Ga, they estimate that Jasperlites (which, as stated in the text, are considered to be altered siderites) to constitute 14% of the sedimentary shell of $25,000 \times 10^{20}$ gr, or 3.0×10^{21} mol $FeCO_3$. Incorporating models for sediment recycling results in an even larger estimate of 22%, as discussed by Garrels and Mackenzie (25). In fact, the large increase in Jasperlites followed by their total disappearance in the phanerozoic is perhaps one of the most remarkable features of Ronov et al's data, as already pointed out by Garrels and Mackenzie (25). Garrels and Perry (4) give a value of 350 Emol of sedimentary $FeCO_3$, though this estimate is based on the amounts required to balance oxidized sedimentary iron rather than by rock data. Nonetheless, their logic holds, and the much larger estimates for oxidized iron which include iron in crystalline silicate rocks correspond very well to the total estimated the mass of siderite available for oxidation at 2.3 Ga.

How did such large amounts of oxidized iron accumulate in the crust? During the Archean iron was likely delivered in reduced form from the weathering of silicate rocks and the dissolution of pyrite and siderite in sedimentary rocks. It likely exited the ocean in equally reduced form as pyrite and siderite. Ferric to total iron ratios in shales are not much different from mantle values until the Great Oxidation Event (38) and it is only following during it that the ferric iron content of shales rises substantially. During the Lomagundi Event pO$_2$ rose to significant levels for the first time and reduced iron delivered from weathering became oxidized on land for the first time. The weathered iron accumulated as oxidized iron in shales and as redbeds on the con-

tinents (redbeds make their first appearance following the Great Oxidation Event). In addition, diagenetic alteration of reduced iron as oxidizing fluids flowed through sedimentary basins for the first time likely also led to substantial accumulation of iron oxides (39). Oxidation of iron in mid-ocean ridge basalts by oceanic sulfate (which likely rose from very low Archean levels for the first time) likely also contributed to growth of the oxidized iron reservoir. The iron in oceanic basalts undergoing subduction would have been particularly likely to be incorporated into crystalline rocks of the continental crust. During the remainder of the Proterozoic, following the Lomagundi Event, weathering would have delivered both oxidized iron and reduced iron. The fraction of iron that in reduced form was likely oxidized subaerially. Some of that iron accumulated as redbeds while some of it was delivered to the marine realm where it was likely reduced and exited as pyrite. This situation likely persisted until oxidation of the deep ocean, much later, during the Phanerozoic, which led to an additional loci of iron oxide deposition in deep sea.

Comparing the values computed according to Equation 10, and the estimated sizes of the crustal reservoirs, in particular of organic carbon, oxidized iron, and sulfate, given in Table S3, shows that the lower estimates (corresponding to a lower duration of the Lomagundi Event and/or lower estimates for total carbon input) match reasonably well to the existing crustal reservoirs. Moreover, the larger estimates for organic carbon, though they exceed the estimates for the *current* reservoirs, do not invalidate the conclusions, as material could have been lost since the Lomagundi Event. For instance, subduction of organic carbon or its oxidation subsequently to the Lomagundi Event could have led to a smaller fraction of the produced organic carbon being preserved. In particular, the hypothesis that subduction of organic carbon as well as its oxidation to methane were accelerated during and immediately following the Lomagundi Event is an attractive one, as it would explain the unidirectional and permanent nature of the Earth surface oxidation that occurred in association with it.

19

Many workers have highlighted the fact that Earth has an excessively oxidized atmosphere and crust. In particular, Lovelock (27, 28) pointed out that while Mars and Venus are at the equilibrium redox potential appropriate to their stations in the solar system, that of Earth is far more oxidized than its position would suggest. The implication is that Earth's unique features, plate tectonics and life, are likely responsible for its current redox state (see also Hayes and Waldbauer, 7). This process was very likely aided by a methane "hydrogen balloon" (Lovelock and Lodge (27), Catling et al. (29)) which transported hydrogen to the upper atmosphere. We suggest that the processes of hydrogen loss to space and to the mantle may have been pulsed as well, and tightly coupled to episodes of organic carbon production (and burial). Thus, the oxidized products accumulated in the crust and atmosphere, while the reducing power was transferred to organic carbon, and then subsequently subducted into the mantle and lost to space. It is worth emphasizing the main difference between our own interpretation of the carbon cycle and that of Hayes and Waldbauer, and others before them, is that while they postulate that the accumulation of oxidants (Fe^{3+}, SO_4^{2-}, O_2) and reductants (C_{org}, FeS_2) occurred gradually throughout the Geozoic, we acknowledge the possibility that large portions of these reservoirs could have been accumulated, and destroyed, in shorter periods of geologic time (on the order of tens to hundreds of millions of years).

S7 Model Description

The model includes mass boxes for the oceanic concentrations of carbon, calcium, sulfur, phosphate, oxygen, and alkalinity, as well as isotopic mass for carbon, calcium and sulfate (Figure S4). The sedimentary reservoirs included in the model are organic carbon, carbonate carbon, sulfide sulfur, sulfate sulfur, reduced iron, and siderite. A carbonate system solver, modified from Emerson and Hedges (30) and Zeebe and Wolf-Gladrow (31), is used to calculate pCO$_2$,

pH, and the carbonate saturation state (Ω) from values of alkalinity and DIC at every model timestep. Complete list of constitutive equations and flux relations is given in Section S8. The full code is supplied in supplemental files.
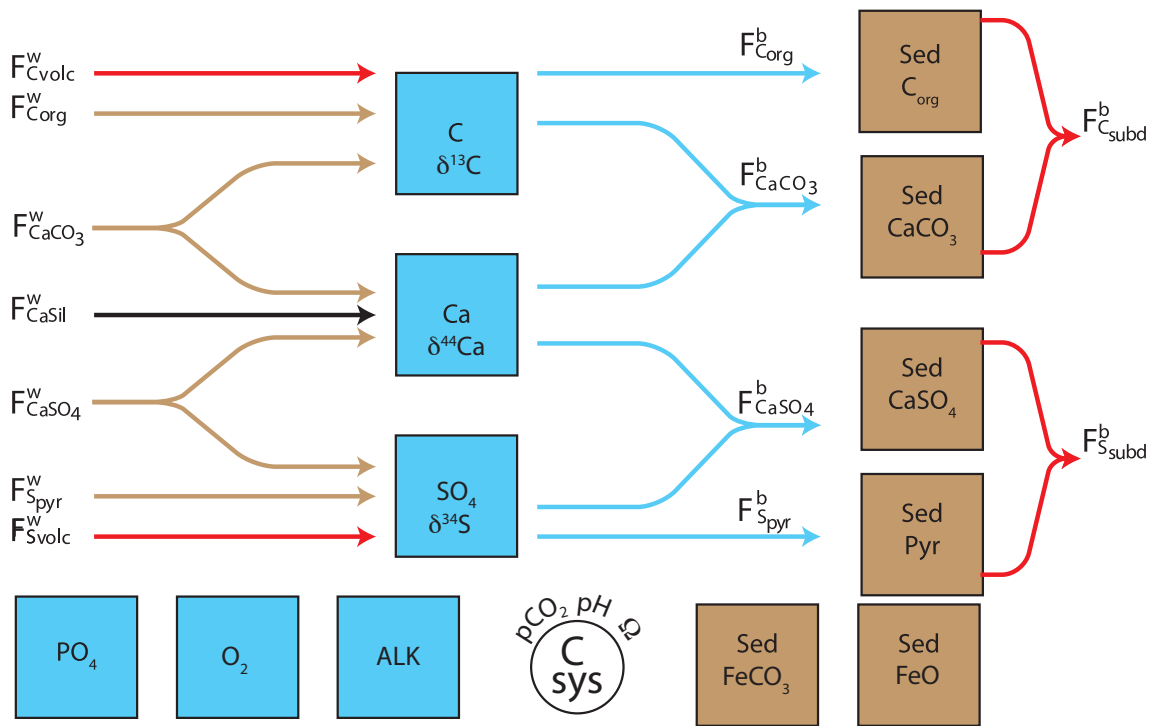

Figure S4: Sketch of model setup. Oceanic and atmospheric reservoirs in blue, sedimentary reservoirs in brown. Burial fluxes from the ocean in blue, weathering fluxes in brown, subduction fluxes and volcanic fluxes in red. C_{sys} stands for carbonate system solver.

The first numerical experiment we perform is a simple sanity test: we force the model with weathering fluxes of siderite, sulfide, and carbonate, and burial of organic carbon and sulfate, in stochiometric relations according to Equation 9 in the main text, such that a +10 permil excursion results. This perturbation is a "Goldilocks" solution with the reactants and products exactly balanced so should incur no changes in pO_2 or pCO_2. Results are shown in Figure S5. In Table S4 we give the values produced by the model, calculated in two ways: firstly, by integrating the relevant fluxes with respect to time, and secondly by subtracting the initial

	Duration	FeS_2	$CaCO_3$	$FeSiO_3$	$FeCO_3$	Fe_2O_3	$CaSO_4$	CH_2O	α
Model Int	100 my	-249.44	-498.89	0	-582.03	415.74	498.89	1080.92	0
Model Sub	100 my	-249.44	-498.88	0	-582.03	415.74	498.88	1080.92	0
Calc	100 my	-249.06	-498.11	0	-581.13	415.09	498.11	1079.24	0

Table S4: Table comparing model output to analytical calculations. First row (Model Int) is obtained by integrating the time-varying fluxes in the model. The second row is obtained by subtracting initial and final sedimentary reservoir sizes. The third row (Calc) are the same values given in Table S3 (5th row: 50 Tmol/yr, 100 m.y.) but without rounding. Nearly identical solutions between the first and second rows indicate that the model conserves mass. Nearly identical solutions of the semi-analytical calculation and numerical model indicate that the model is accurate.

and final sedimentary reservoir masses. The differences between the first row (integration) and second row (subtraction) are in the second decimal point, indicating that the model preserves mass. The differences between the model and the calculation arise due to truncation error, as well as the maximal $\delta^{13}C$ in the model, which is 10.001‰, as opposed to an exact 10‰ in the calculation. The differences are on the order of 0.15% of the analytical solution, indicating that the model is reasonably accurate.

The next numerical experiment we perform is to incorporate parameterizations for the weathering and burial fluxes, and force a pulse of organic carbon burial. We first force the model without any pyrite oxidation, and we then add two different parameterizations of the pyrite oxidation flux. We show the model outputs for $\delta^{13}C$, pCO_2, and pO_2 in Figure S6.

The model results are that under the scenario of pyrite oxidation according to the Williamson and Rimstidt parameterization (green dashed line) pCO_2 falls to 46.6 ppm. Under the scenario where the pyrite and gypsum weathering fluxes are set to the modern ones with modification for the reservoir size (blue solid line), pCO_2 falls the least, but still reaches very low values of 108.3 ppm. The decline in pCO_2 is driven by the burial of organic carbon: the removal of DIC from ocean water, with little accompanying alkalinity, drives the carbonate system from neutrality and towards a zone of higher pH and lower pCO_2. The weathering fluxes, which are
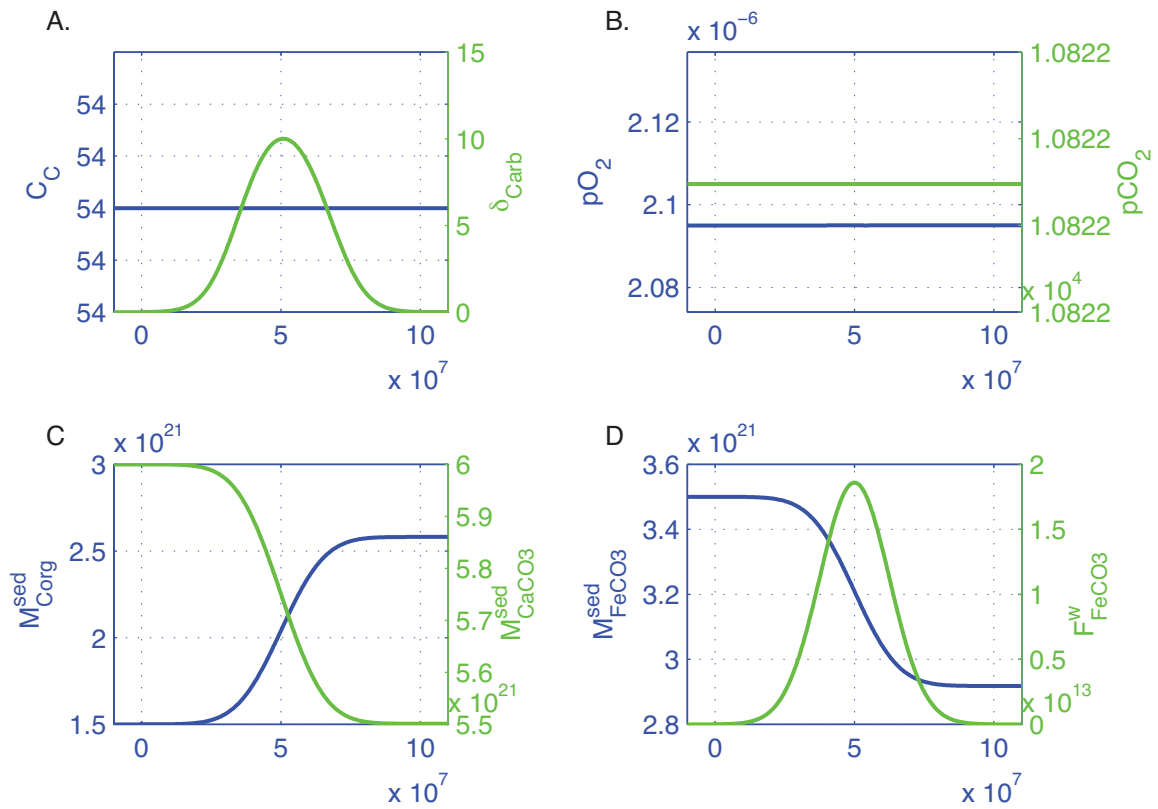
22

Figure S5: Model outputs for a pulse of carbon burial coupled to carbonate carbon acidification, sulfide oxidation, and siderite oxidation in accordance with Equation 9 in the main text, such that a +10 permil excursion results. This perturbation does not result in changes in pO_2 or pCO_2 since it follows a stoichiometrically balanced reaction for both species. A. The concentration of inorganic carbon in the ocean (C_C) and its isotopic composition (δ_{Carb}). B. Atmospheric oxygen and carbon dioxide concentrations (pO_2, pCO_2) C. Mass of sedimentary organic carbon and carbonate carbon reservoirs (M_{Corg}^{sed} and M_{Ccarb}^{sed}). D. Mass of siderite and the siderite oxidation flux (M_{FeCO3}^{sed} and F_{FeCO3}^{W}).
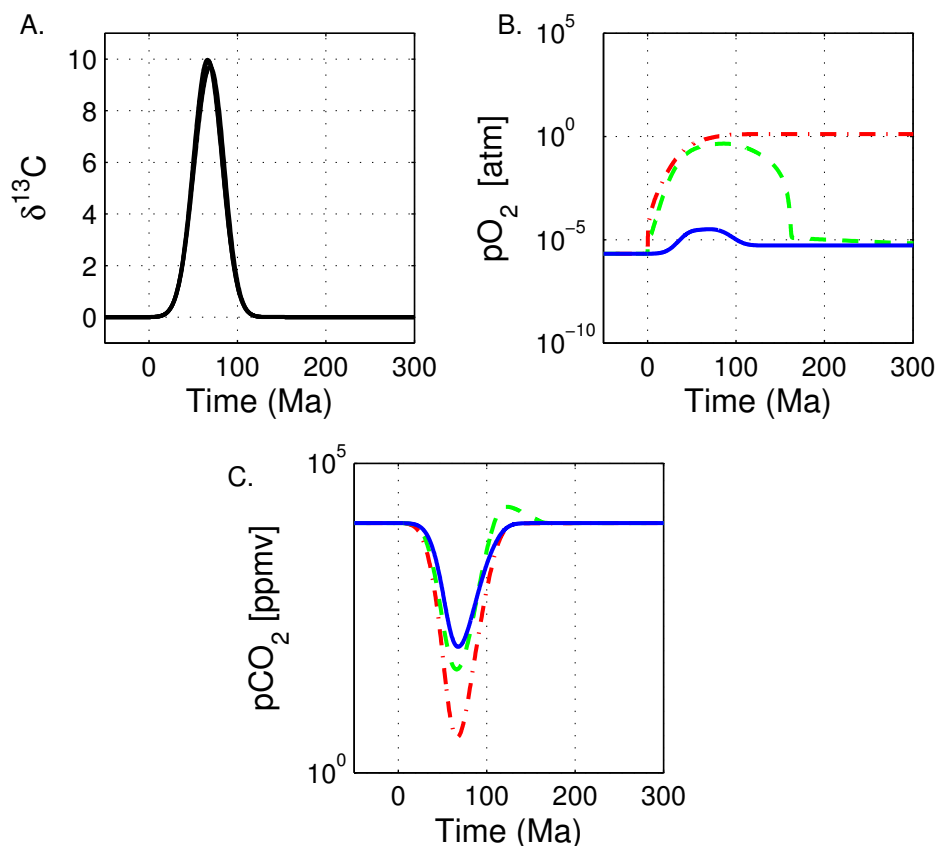
Figure S6: Model outputs for a pulse of carbon burial unaccompanied by increased carbon input. All simulations show a drop in $p\mathrm{CO_2}$ to extremely low levels. Under the scenario of no pyrite oxidation (red dash-dotted line) $p\mathrm{CO_2}$ falls to 3.76 ppm, close to the theoretical value calculated in Table S1. Under the scenario of pyrite oxidation according to the Williamson and Rimstidt parameterization (green dashed line) $p\mathrm{CO_2}$ falls to 46.6 ppm. Under the scenario where the pyrite and gypsum weathering fluxes are set to the modern ones with modification for the reservoir size (blue solid line), $p\mathrm{CO_2}$ falls the least, but still reaches very low values of 108.3 ppm. The inclusion of pyrite oxidation impacts the $p\mathrm{O_2}$ response as well. Without pyrite oxidation, oxygen accumulates and remains high, whereas with pyrite oxidation, $p\mathrm{O_2}$ returns to baseline after the perturbation. The peak values for $p\mathrm{O_2}$ are 0.46 atm (2.1 PAL) under the Williamson and Rimstidt parameterization, and 3×10^{-5} (3x baseline) under the alternative parameterization. Note log scale on y axes in B. and C.

set to be proportional to $p\text{CO}_2{}^{0.3}$, respond by declining, thus lowering the input of carbon and alkalinity from weathering. The carbonate burial flux, which is proportional to the carbonate saturation state, declines as well, even as pH increases, because of the reduction in the input of Ca^{2+}. The system thus approaches a new equilibrium, one in which the inputs of alkalinity are equal to the much reduced outputs of alkalinity. When sulfide oxidation is added to the model weathering fluxes, the contribution of sulfate helps mitigate the imbalance in alkalinity, thus resulting in higher $p\text{CO}_2$ levels. The oxidation of pyrite also leads to a more realistic behavior of O_2, whereby instead of accumulating in the atmosphere and remaining constant after the perturbation, O_2 returns to steady-state after the perturbation (compare dash-dotted curve to the dashed and solid lines in Figure S6.B).

Since the parameterization of the pyrite oxidation flux exerts such a strong control on the $p\text{CO}_2$ and $p\text{O}_2$ response of the model during the positive excursion, a brief description of the available choices is in order. The first, simpler yet probably less appropriate parameterization, is one that takes the current modern estimates and scales them to the size of the Late Archean - Early Proterozoic sulfate and sulfide sedimentary reservoirs, which were likely much smaller and much larger, respectively. Thus, if the Phanerozoic estimates for the sulfide and sulfate sedimentary reservoirs are 294 and 240 Emol (a ratio of 0.55), and associated fluxes are 0.93 and 0.76 Tmol S /yr (using the values from Garrels and Perry, 4), then assuming a 0.99 ratio of sedimentary reservoir masses in favor of sulfide gives fluxes of 1.72 and 0.01 Tmol S /yr for the Late Archean - Early Proterozoic. We allow the sulfide oxidation flux to scale as the square root of the ratio of $p\text{O}_2$ to its initial value, and linearly with the size of the remaining pyrite reservoir:

$$\text{F}^{\text{w}}_{\text{FeS2}} = \text{F}^{\text{w,i}}_{\text{FeS2}} * \left[\frac{p\text{O}_2}{p\text{O}_{2,\text{i}}}\right]^{0.5} * \left[\frac{\text{M}^{\text{sed}}_{\text{FeS2}}}{\text{M}^{\text{sed}}_{\text{FeS2,i}}}\right] \tag{S43}$$

The alternative formulation takes into account the kinetics of pyrite oxidation as experimentally

constrained by Williamson and Rimstidt (32) (see also Bolton et al., 33):

$$R_{FeS_2} = \frac{10^{-8.19} \left[pO_2 * K_H^{O2} \right]^{0.5}}{[H^+]^{0.11}} * 31536000; \tag{S44}$$

where R_{FeS_2} is the rate at which pyrite is oxidized with units of $[\frac{mol}{m^2\,yr}]$ (the factor of 31536000 converts from seconds to years). It is observed to scale with the square root of the dissolved aqueous O_2 concentration (which is given by atmospheric O_2 multiplied by Henry's constant for oxygen, 0.00126 [mol/L/Atm at 25C]), and to be weakly inversely proportional (0.11 power) to the concentration of protons in the weathering solution, which we calculate as pH of pristine rainwater in equilibrium with atmospheric CO_2, which is given as the roots of a cubic equation in $[H^+]$ (Harte (34), Stumm and Morgan (35)):

$$[H^+]^3 - [pCO_2 * k_1 * k_H + k_w] * [H^+] - 2 * (pCO_2 * k_2 * k_1 * k_H) \tag{S45}$$

with the appropriate rate constants: $k_H = 10^{-1.47}$, $k_1 = 10^{-6.35}$, $k_2 = 10^{-10.33}$, $k_w = 10^{-14}$. Once the oxidation rate is known, a scaling relationship between the calculated rate of pyrite oxidation under modern pCO_2 and pO_2 conditions ($R_{FeS_2}^{mod}$), and the estimated modern pyrite oxidation flux ($F_{FeS2}^{w,mod}$) and reservoir size ($M_{FeS2}^{sed,mod}$) can be obtained:

$$K_{Pyr}^{ox} = \frac{F_{FeS2}^{w,mod}}{R_{FeS_2}^{mod} * M_{FeS2}^{sed,mod}} \tag{S46}$$

This constant (K_{Pyr}^{ox}) can then by used to calculate the pyrite oxidation flux under different boundary conditions of reservoir size and oxidation rate (as a function of pO_2 and pCO_2):

$$F_{FeS2}^{w} = K_{Pyr}^{ox} * R_{FeS_2} * M_{FeS2}^{sed}; \tag{S47}$$

The result of scaling to a higher pCO_2, lower pO_2, and larger reservoir size, is that pyrite oxidation is calculated to be substantially smaller in the low-O_2 Archean (approximately $1x10^9$ Tmol/yr versus $1x10^{11}$ Tmol/yr in the present). The initial magnitude of the sulfide oxidation flux under the different parameterizations ($4.47x10^9$ or $1.67x10^{12}$ Tmol/yr) makes a difference

410 for how high $p\mathrm{O}_2$ needs to go up to increase the flux such that it balances the accumulation of

411 alkalinity due to organic carbon burial. The higher the initial value, the less $p\mathrm{O}_2$ has to increase

412 in order to balance the input and outputs of carbon and alkalinity. Nonetheless, because of the

413 inherent imbalances associated with pyrite oxidation, which lead to a shortage of carbon, $p\mathrm{CO}_2$

414 falls to low levels, irrespective of the parameterization used.

415 Next, we perturb the model with a Gaussian shaped excess organic carbon burial flux, and allow

416 for siderite and iron silicate oxidation, in addition to pyrite oxidation. The results are shown

417 in Figure S7. With increasing siderite contribution the $p\mathrm{O}_2$ peak increases, the $p\mathrm{CO}_2$ minimum

418 rises, and the $p\mathrm{CO}_2$ maximum becomes more pronounced. In the first case (red dash-dotted

419 line) with 813 Emol of FeCO_3 consumed $p\mathrm{CO}_2$ falls to 2800 ppm and then rises 13,600 ppm.

420 In the second case (green dashed line) with 1118 Emol of FeCO_3 consumed $p\mathrm{CO}_2$ falls to 7600

421 ppm and then rises 16,500 ppm. In the third case (blue solid line) with 1424 Emol of FeCO_3

422 consumed $p\mathrm{CO}_2$ is not reduced at all and then rises 21,150 ppm. Perhaps counter-intuitively,

423 the increasing amount of siderite causes the $p\mathrm{CO}_2$ peak associated with the declining limb of

424 the $\delta^{13}\mathrm{C}$ excursion to be smaller. This is because the oxidation of siderite (and iron silicates)

425 diverts O_2 from sulfide oxidation, and it is the sulfide oxidation flux which drives the increase

426 in $p\mathrm{CO}_2$ through its effects on alkalinity and thus carbonate burial. A higher sulfide oxidation

427 flux leads to a smaller carbonate burial flux because of the sulfide oxidation's contribution of

428 acidity, and hence a larger imbalance which then is required to correct itself, leading to a $p\mathrm{CO}_2$

429 overshoot.

430 We show the changes in $[\mathrm{SO}_4]$ and $\delta^{34}\mathrm{S}$ of the oceanic sulfate box associated with each of

431 these three model runs in Figure S8 and Figure S9. The resulting trends in $\delta^{34}\mathrm{S}$, as stated

432 in the main text, arise mainly due to two effects. The sharp rise and decline in $\delta^{34}\mathrm{S}$ are a

433 result of increased fractionation associated with increased availability of sulfate. We use the
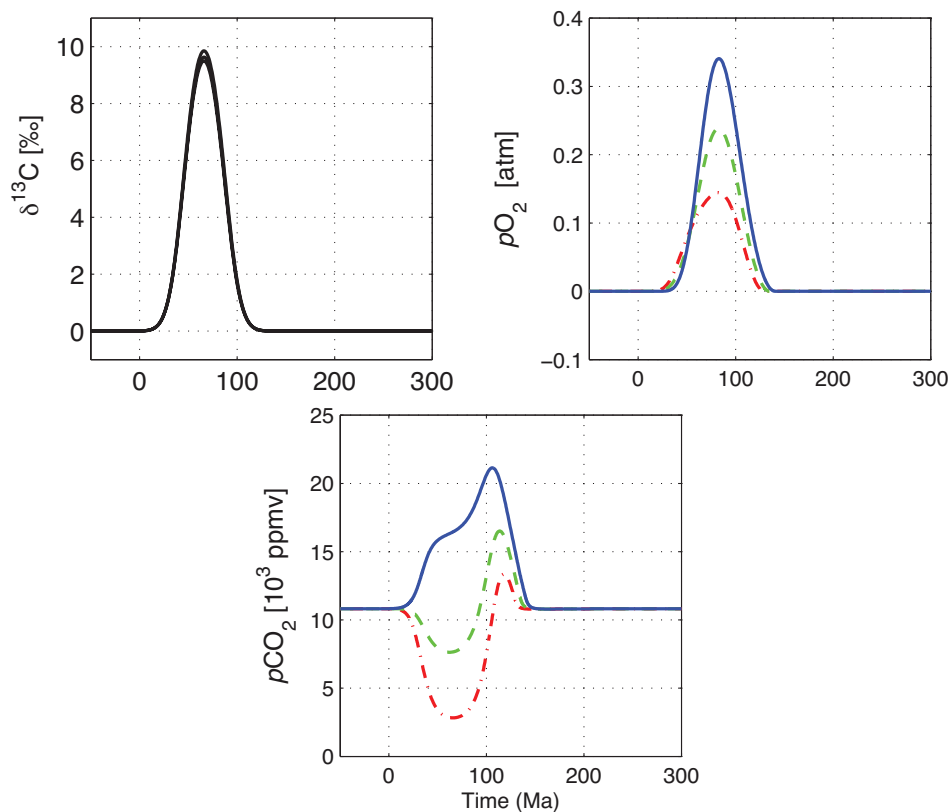
Figure S7: Model outputs for a pulse of carbon burial accompanied by siderite, pyrite, and iron silicate oxidation. With increasing siderite contribution the pO_2 peak increases, the pCO_2 minimum rises, and the pCO_2 maximum becomes more pronounced. In the first case with a low amount of siderite oxidized (red dash-dotted line) pCO_2 falls to 2800 ppm and then rises 13600 ppm, and pO_2 rises to 0.14 Atm. In the second case with an intermediate amount of siderite oxidized (green dashed line) pCO_2 falls to 7600 ppm and then rises 16500 ppm, and O_2 rises to 0.23 Atm. In the third case with a large amount of siderite oxidized (blue solid line) pCO_2 is not reduced at all and then rises 21150 ppm, while pO_2 rises to 0.34 Atm.
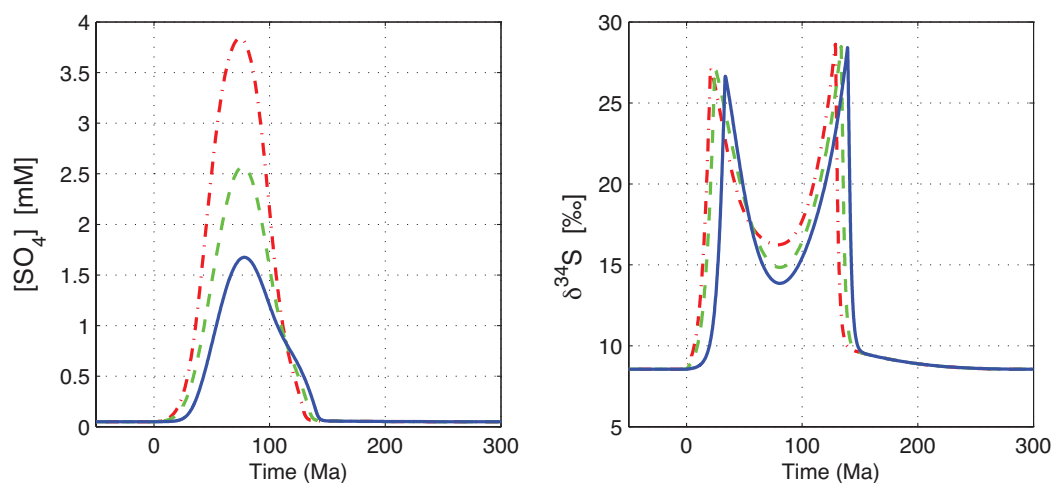
Figure S8: Variation in the [SO$_4$] and δ^{34}S of the oceanic sulfate box, same model runs as in Figure S7 above.

parameterization suggested by Habicht et al. (36), with a fractionation factor of 1.029 above a threshold of 190 μM and a linear decrease to 1.000 as sulfate decreases towards zero. Since all model runs include a rise in SO$_4$ above 190 μM there is little variation in the response with varying pyrite oxidation rates. In contrast, the drop in δ^{34}S in the middle is a result of the influx of light sulfide to the sulfate box from pyrite oxidation, and some variation is apparent: lower δ^{34}S result from increased sulfate input. As shown in Figure S9 and in the main text these results fit the data from Planavsky et al. (37) quite well, lending support to our interpretation of the events which occurred during Lomagundi times.
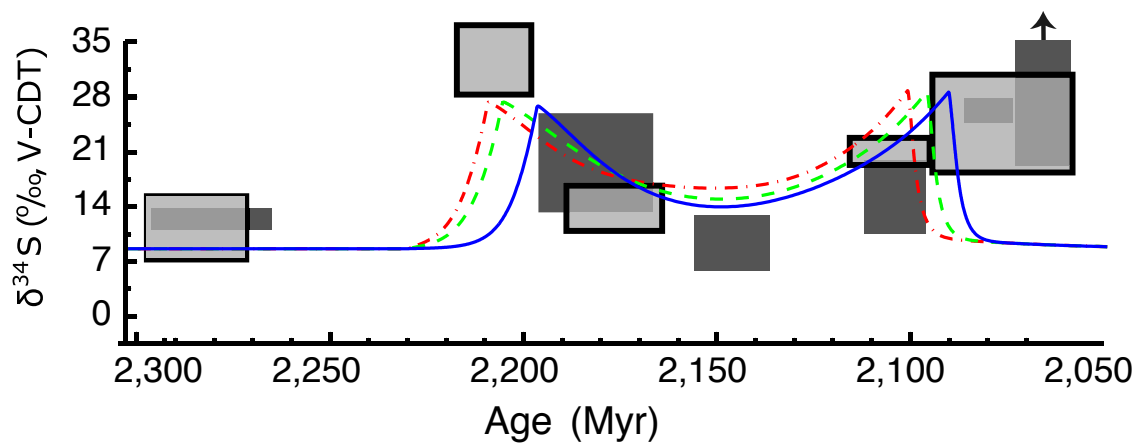
29

Figure S9: Plot of modeled δ^{34}S variation overlaying data from Planavsky et al. (37). In the model the sharp rise and fall in δ^{34}S are a result of increased fractionation associated with increased availability of sulfate, while the drop in δ^{34}S in the middle is a result of the influx of light sulfide to the sulfate box from pyrite oxidation. Lines are the same model runs as in Figures S7 and S8.

S8 Model Equations

Table S5: Steady-state values for model fluxes and reservoirs

Description	Name	Value	Unit
Dissolved inorganic carbon	DIC	$54.0 \cdot 10^{-3}$	mol/kg
Dissolved calcium	Ca	$0.13 \cdot 10^{-3}$	mol/kg
Alkalinity	ALK	$58.5 \cdot 10^{-3}$	eq/kg
Dissolved phosphate	PO_4	$0.25 \cdot 10^{-6}$	mol/kg
Partial pressure of CO_2	pCO_2	10822	ppmv
Calcite Saturation	Ω	1.45	-
pH	ph	8.03	-
Steady-state volcanic input	F_{volc}	$5 \cdot 10^{12}$	mol/yr
Weathering input of organic carbon	F^w_{org}	$9 \cdot 10^{12}$	mol/yr
Weathering input of $CaCO_3$	F^w_{carb}	$36 \cdot 10^{12}$	mol/yr
Silicate weathering input of calcium	F^w_{sil}	$4 \cdot 10^{12}$	mol/yr
Weathering input of phosphate	F^w_p	$9.3 \cdot 10^{10}$	mol/yr
Burial of organic carbon	F^b_{org}	$10 \cdot 10^{12}$	mol/yr
Burial of $CaCO_3$	F^b_{carb}	$40 \cdot 10^{12}$	mol/yr
Burial of phosphate	F^b_p	$9.3 \cdot 10^{10}$	mol/yr
C:P burial ratio	CP	106	-
$\delta^{13}C$ of volcanic flux	δ_{volc}	-5	permil
$\delta^{13}C$ of carbonate weathering	δ^w_{carb}	0	permil
$\delta^{13}C$ of organic carbon weathering	δ^w_{org}	-25	permil
$\delta^{13}C$ of carbonate burial	δ	0	permil
$\delta^{13}C$ of organic carbon weathering	δ^b_{org}	-25	permil
Photosynthetic fractionation	ϵ	25	permil

Flux values after DePaolo (40) and Kump and Arthur (1). Magnitude of photosynthetic fractionation from Hayes et al. (41). Concentrations of carbon, calcium, and phosphate converted to masses using an ocean volume of $1.32 \cdot 10^{21}$ L and salinity of 1.035 kg/L.

Table S6: Isotopic mass equations for oceanic reservoirs

$$\frac{dM_C}{dt} = F^w_{C_{volc}} + F^w_{CaCO_3} + F^w_{C_{org}} - F^b_{C_{org}} - F^b_{C_{carb}} \tag{S48}$$

$$\frac{dM_{Ca}}{dt} = F^w_{Ca_{sil}} + F^w_{CaCO_3} + F^w_{CaSO_4} - F^b_{CaCO_3} - F^b_{CaSO_4} \tag{S49}$$

$$\frac{dM_{PO_4}}{dt} = F^w_{PO_4} - F^b_{PO_4} \tag{S50}$$

$$\frac{dM_S}{dt} = F^w_{S_{volc}} + F^w_{CaSO_4} + F^w_{Pyr} - F^b_{CaSO_4} - F^b_{Pyr} \tag{S51}$$

$$\frac{dO_2}{dt} = F^b_{C_{org}} + 1.875\, F^b_{Pyr} - F^w_{C_{org}} - 1.875\, F^w_{Pyr} - f^{redox}_{volc_C}\, F^w_{C_{volc}} \tag{S52}$$

$$- 1.875\, f^{redox}_{volc_S}\, F^w_{S_{volc}} \tag{S53}$$

$$\frac{d\delta_C}{dt} = \left[F^w_{C_{volc}}(\delta_{C_{volc}} - \delta_C) + F^w_{CaCO_3}(\delta^w_{CaCO_3} - \delta_C) \right.$$

$$\left. + F^w_{org}(\delta^w_{org} - \delta_C) - (F^b_{org})(-\epsilon_C) \right] \frac{1}{M_C} \tag{S54}$$

$$\frac{d\delta_{Ca}}{dt} = \left[F^w_{Ca_{sil}}(\delta^w_{Ca_{sil}} - \delta_{Ca}) + F^w_{CaCO_3}(\delta^w_{Ca_{carb}} - \delta_{Ca}) \right.$$

$$\left. + F^w_{CaSO_4}(\delta^w_{Ca_{sulf}} - \delta_{Ca}) - (F^b_{CaCO_3} + F^b_{CaSO_4})(-\epsilon_{Ca}) \right] \frac{1}{M_{Ca}} \tag{S55}$$

$$\frac{d\delta_S}{dt} = \left[F^w_{S_{volc}}(\delta_{S_{volc}} - \delta_S) + F^w_{CaSO_4}(\delta^w_{Sulf} - \delta_S) + F^w_{Pyr}(\delta^w_{Pyr} - \delta_S) \right.$$

$$\left. - F^b_{Pyr}(-\epsilon_S) \right] \frac{1}{M_S} \tag{S56}$$

Table S7: Mass and isotopic mass equations for sedimentary reservoirs

$$\frac{dM_{S_{pyr}}^{sed}}{dt} = F_{Pyr}^{b} - F_{Pyr}^{w} - F_{S_{Pyr}}^{subd} \tag{S57}$$

$$\frac{dM_{S_{sulf}}^{sed}}{dt} = F_{CaCO_3}^{b} + F_{CaSO_4}^{b} - F_{CaSO_4}^{w} - F_{S_{sulf}}^{subd} \tag{S58}$$

$$\frac{dM_{C_{org}}^{sed}}{dt} = F_{C_{org}}^{b} - F_{C_{org}}^{w} - F_{C_{org}}^{subd} \tag{S59}$$

$$\frac{dM_{CaCO_3}^{sed}}{dt} = F_{CaCO_3}^{b} - F_{CaCO_3}^{w} - F_{CaCO_3}^{subd} \tag{S60}$$

Table S8: Weathering feedbacks

$$F_{Ca_{sil}}^{w} = F_{Ca_{sil}}^{w} \cdot \left(R_{CO_2}\right)^{0.3} \tag{S61}$$

$$F_{CaCO_3}^{w} = F_{CaCO_3,i}^{w} \cdot \left(R_{CO_2}\right)^{0.3} \tag{S62}$$

$$F_{C_{org}}^{w} = F_{C_{org},i}^{w} \cdot \left(R_{CO_2}\right)^{0.3} \tag{S63}$$

$$F_{PO_4}^{w} = F_{PO4,i}^{w} \cdot \left(R_{CO_2}\right)^{0.3} \tag{S64}$$

Table S9: Sulfide oxidation feedbacks

$$[H^+] = \text{roots}(\, [H^+]^3 - [pCO_2 * k_1 * k_H + k_w] * [H^+] - 2 * (pCO_2 * k_2 * k_1 * k_H) \,) \quad \text{(S65)}$$

$$k_H = 10^{-1.47}, \ k_1 = 10^{-6.35}, \ k_2 = 10^{-10.33}, \ k_w = 10^{-14} \quad \text{(S66)}$$

$$R_{FeS_2} = \frac{10^{-8.19} \, (\, pO_2 * K_H^{O2} \,)^{0.5}}{[H^+]^{0.11}} * 31536000; \quad \text{(S67)}$$

$$K_{Pyr}^{ox} = \frac{F_{FeS2}^{w,mod}}{R_{FeS_2}^{mod} * M_{FeS2}^{sed,mod}} \quad \text{(S68)}$$

$$F_{FeS2}^{w} = K_{Pyr}^{ox} * R_{FeS_2} * M_{FeS2}^{sed}; \quad \text{(S69)}$$

Table S10: Burial feedbacks

$$F_{CaCO_3}^{b} = F_{CaCO_3,i}^{b} \cdot \left(\frac{\Omega_{CaCO_3}}{\Omega_{CaCO_3,i}} \right) \quad \text{(S70)}$$

$$F_{CaSO_4}^{b} = F_{CaSO_4}^{b} \cdot \left(\frac{ICP_{CaSO_4}}{ICP_{CaSO_4,i}} \right) \quad \text{(S71)}$$

$$F_{PO_4}^{b} = F_{PO_4,i}^{b} \cdot \left(\frac{M_{PO_4}}{M_{PO_4,i}} \right) \quad \text{(S72)}$$

Table S11: Auxiliary definitions

$$\Omega_{\text{CaCO}_3} = \frac{[\text{Ca}] \cdot [\text{CO}_3^=]}{\text{k}_{\text{calcite}}^{\text{sat}}} \quad \text{(S73)}$$

$$\text{ICP}_{\text{CaSO}_4} = [\text{Ca}] \cdot [\text{SO}_4] \quad \text{(S74)}$$

$$[\text{ALK}] = 2[\text{Ca}] - 2[\text{SO}_4] + 2[\text{Mg}] + [\text{K}] + [\text{Na}] - [\text{Cl}] \quad \text{(S75)}$$

$$\text{R}_{\text{CO}_2} = \frac{\text{pCO}_2}{\text{pCO}_{2,\text{i}}} \quad \text{(S76)}$$

$$\text{(S77)}$$

References

[1] Kump, L. R & Arthur, M. A. (1999) Interpreting carbon-isotope excursions: carbonates and organic matter. *Chemical Geology* **161**, 181 – 198.

[2] Torres, M. A, West, A. J, & Li, G. (2014) Sulphide oxidation and carbonate dissolution as a source of CO_2 over geological timescales. *Nature* **507**, 346–349.

[3] MATLAB, version R2009a. The MathWorks Inc., Natick, Massachusetts.

[4] Garrels, R & Perry, E. (1974) *Cycling of carbon, sulphur and oxygen through geologic time*, The sea: ideas and observations on progress in the study of the seas. (J. Wiley, New York) Vol. 5, pp. 303–336.

[5] Sleep, N. H. (2004) Dioxygen over geological time. *Metal ions in biological systems* **43**, 49–73.

[6] Holser, W, Schidlowski, M, Mackenzie, F, & Maynard, J. (1988) Geochemical cycles of carbon and sulfur. *Chemical Cycles in the Evolution of the Earth* pp. 105–173.

[7] Hayes, J. M & Waldbauer, J. R. (2006) The carbon cycle and associated redox processes through time. *Philosophical Transactions of the Royal Society B: Biological Sciences* **361**, 931–950.

[8] Yaroshevsky, A. (2006) Abundances of chemical elements in the Earth's crust. *Geochemistry International* **44**, 48–55.

[9] Ronov, A, Migdisov, A, & Yaroshevsky, A. (1970) *The main stages of geochemical history of the outer shells of the Earth*. (Clarke Cy Washington, DC), pp. 40–53.

[10] Holser, W & Kaplan, I. (1966) Isotope geochemistry of sedimentary sulfates. *Chemical Geology* **1**, 93–135.

[11] Li, Y.-H. (1972) Geochemical mass balance among lithosphere, hydrosphere, and atmosphere. *Am. J. Sci* **272**, 119–137.

[12] Schidlowski, M & Eichmann, R. (1977) *Evolution of the terrestrial oxygen budget*, ed. Ponnamperuma, C. (Academic Press, New York), pp. 87–89.

[13] Nielsen, H. (1979) in *Lectures in isotope geology*. (Springer), pp. 283–312.

[14] Garrels, R. M & Lerman, A. (1981) Phanerozoic cycles of sedimentary carbon and sulfur. *Proceedings of the National Academy of Sciences* **78**, 4652–4656.

[15] Wedepohl, K. H. (1995) The composition of the continental crust. *Geochimica et Cosmochimica Acta* **59**, 1217 – 1232.

[16] Hunt, J. (1995) *Petroleum Geochemistry and Geology*. (W. H. Freeman., New York), 2nd edition.

[17] Des Marais, D. J. (2001) Isotopic evolution of the biogeochemical carbon cycle during the Precambrian. *Reviews in Mineralogy and Geochemistry* **43**, 555–578.

[18] Berner, R. (2004) *The Phanerozoic carbon cycle: CO_2 and O_2*. (Oxford University Press).

[19] Arvidson, R. S, Mackenzie, F. T, & Guidry, M. (2006) MAGic: A Phanerozoic model for the geochemical cycling of major rock-forming components. *American Journal of Science* **306**, 135–190.

[20] Wilkinson, B. H & Walker, J. C. (1989) Phanerozoic cycling of sedimentary carbonate. *American Journal of Science* **289**, 525–548.

[21] Vinogradov, A. (1962) Average contents of chemical elements in the principal types of igneous rocks in the Earth's crust [in russian]. *Geokhimiya*.

[22] Ronov, A, Yaroshevskii, A, & Migdisov, A. (1990) *Chemical structure of the Earth's srust and geochemical balance of major elements [in Russian]*.

[23] Ronov, A & Yaroshevsky, A. (1976) A new model for the chemical structure of the Earth's crust. *Geochem. Int* **13**, 89–121.

[24] Ohmoto, H, Watanabe, Y, & Kumazawa, K. (2004) Evidence from massive siderite beds for a CO_2-rich atmosphere before~ 1.8 billion years ago. *Nature* **429**, 395–399.

[25] Garrels, R. M & Mackenzie, F. T. (1971) *Evolution of sedimentary rocks*. (W.W. Norton & Company, Inc.).

[26] Veizer, J. (1978) Secular variations in the composition of sedimentary carbonate rocks, II. Fe, Mn, Ca, Mg, Si and minor constituents. *Precambrian Research* **6**, 381–413.

[27] Lovelock, J. E & Lodge Jr, J. P. (1972) Oxygen in the contemporary atmosphere. *Atmospheric Environment (1967)* **6**, 575–578.

[28] Lovelock, J. E & Margulis, L. (1974) Atmospheric homeostasis by and for the biosphere: the Gaia hypothesis. *Tellus* **26**, 2–10.

[29] Catling, D. C, Zahnle, K. J, & McKay, C. P. (2001) Biogenic methane, hydrogen escape, and the irreversible oxidation of early Earth. *Science* **293**, 839–843.

[30] Emerson, S & Hedges, J. I. (2008) *Chemical oceanography and the carbon cycle*. (Cambridge University Press).

[31] Zeebe, R. E & Wolf-Gladrow, D. (2001) *CO$_2$ in Seawater - Equilibrium, Kinetics, Isotopes*, Elsevier Oceanography Book Series ed. Halpern, D. (Elsevier, Amsterdam) Vol. 65, p. 346.

[32] Williamson, M. A & Rimstidt, J. D. (1994) The kinetics and electrochemical rate-determining step of aqueous pyrite oxidation. *Geochimica et Cosmochimica Acta* **58**, 5443–5454.

[33] Bolton, E. W, Berner, R. A, & Petsch, S. T. (2006) The weathering of sedimentary organic matter as a control on atmospheric O$_2$: II. Theoretical modeling. *American Journal of Science* **306**, 575–615.

[34] Harte, J. (1988) *Consider a spherical cow: A course in environmental problem solving*. (University Science Books).

[35] Stumm, W & Morgan, J. J. (2012) *Aquatic chemistry: chemical equilibria and rates in natural waters*. (John Wiley & Sons) Vol. 126.

[36] Habicht, K. S, Gade, M, Thamdrup, B, Berg, P, & Canfield, D. E. (2002) Calibration of sulfate levels in the Archean ocean. *Science* **298**, 2372–2374.

[37] Planavsky, N. J, Bekker, A, Hofmann, A, Owens, J. D, & Lyons, T. W. (2012) Sulfur record of rising and falling marine oxygen and sulfate levels during the Lomagundi event. *Proceedings of the National Academy of Sciences* **109**, 18300–18305.

[38] Bekker, A. & Holland, H. (2012) Oxygen overshoot and recovery during the early Paleoproterozoic. *Earth and Planetary Science Letters* **317**, 295–304.

[39] Rasmussen, B., Krapež, B., & Meier, D. B. (2014) Replacement origin for hematite in

2.5 Ga banded iron formation: Evidence for postdepositional oxidation of iron-bearing minerals. *Geological Society of America Bulletin*, **126**,438–446.

[40] DePaolo, D. J. (2004) Calcium isotopic variations produced by biological, kinetic, radiogenic and nucleosynthetic processes. *Reviews in Mineralogy and Geochemistry* **55**, 255–288.

[41] Hayes, J. M, Strauss, H, & Kaufman, A. J. (1999) The abundance of ^{13}C in marine organic matter and isotopic fractionation in the global biogeochemical cycle of carbon during the past 800 Ma. *Chemical Geology* **161**, 103 – 125.